Small

NANO · MICRO small
www.small-journal.com

RESEARCH ARTICLE OPEN ACCESS

Programming Multidomain Peptides With Molecular Frustration Into Biomolecular Condensates

Debdatta Das[1] | Jenny N. Nguyen[1] | Navneet Sahoo[1] | Chuanye Xiong[2] | Haritha Asokan-Sheeja[1] | Yan Chang[3] | Raniyah Ali[1] | Eleanor D. Smith[2] | Chad A. Brautigam[4] | Yi Hong[5] | Zui Pan[3] | Peng Tao[2] | He Dong[1]

[1]Department of Chemistry and Biochemistry, The University of Texas at Arlington, Arlington, Texas, USA | [2]Department of Chemistry, Southern Methodist University, Dallas, Texas, USA | [3]College of Nursing and Health Innovation, The University of Texas at Arlington, Arlington, Texas, USA | [4]Department of Biophysics, The University of Texas Southwestern Medical Center, Dallas, Texas, USA | [5]Department of Bioengineering, The University of Texas at Arlington, Arlington, Texas, USA

Correspondence: He Dong (he.dong@uta.edu)

Received: 9 March 2026 | **Revised:** 22 May 2026 | **Accepted:** 20 June 2026

Keywords: bacterial responsive | beta sheet | biomolecular condensate | complex coacervate | peptide

ABSTRACT

The discovery of biomolecular condensates, driven by liquid–liquid phase separation of intrinsically disordered proteins has significant impacts on both fundamental and applied science and engineering. Although most studies on biomolecular condensates focus on intrinsically disordered structures, research on the role of molecular ordering remains largely unexplored, however is beneficial for gaining new mechanistic understanding and further expand the design space of peptides for constructing functional condensates. Toward this goal, we conducted systematic studies on how molecular ordering impacts the phase behaviors of peptides using multidomain peptides (MDPs) as a model system. MDPs were designed using a molecular frustration principle in which parts of the peptides favored β-sheet assembly and parts favored disassembly. Through programming of each domain, it is evident that the phase behavior of MDPs is largely dictated by the secondary structure, and partially folded β-sheet plays a key role in driving MDPs to form condensates. We also discovered complex coacervates formed by MDPs and synthetic anionic polymers, which exhibited dramatically improved stability. Furthermore, we show enzyme-triggered condensation can be achieved using phosphorylated MDPs as the molecular precursor and alkaline phosphatase as a molecular switch, highlighting the potential of these materials for bacterial imaging and antimicrobial therapy development.

1 | Introduction

Biomolecular condensates, also known as membraneless organelles, have attracted significant interests because of their important roles in regulating numerous essential biochemical processes within cells [1–3]. Natural condensates such as stress granules and nucleoli are formed through liquid-liquid phase separation (LLPS) of intrinsically disordered proteins (IDPs) with or w/o nucleic acids [4–6]. Within these liquid droplets, IDPs and nucleic acids are concentrated via multiple weak non-covalent interactions. The components remain highly dynamic, rapidly exchanging with the surrounding environment, which is crucial for functions such as transient storage of biomolecules and modulation of enzymatic activity [7, 8]. These remarkable characteristics have motivated the creation of synthetic condensates to investigate and understand the mechanisms underlying their formation and function [9–17]. Moreover, synthetic condensates provide significant opportunities for applications in drug delivery, enzymatic microreactors, and the construction of protocell-like systems [18–22].

Compared with recombinant IDPs, peptides provide a minimalist yet highly versatile platform for designing synthetic

condensates [23–29]. Peptides can be synthesized with precisely controlled molecular composition, charge distribution, valency, and secondary structural propensity, which allows a systematic study of the molecular determinants governing phase separation and condensate formation. Additionally, the synthetic versatility through incorporating both natural and non-natural moieties in the primary sequence enables further engineering of condensates with emerging properties for selective partitioning of biomolecules, stimuli-responsiveness, or catalytic functionality [30–32]. Indeed, significant progress has been made by multiple groups elucidating how peptides form self-coacervates and complex coacervates with nucleic acids, highlighting their potential as modular building blocks for synthetic biomolecular condensates [20, 27, 33].

Although most studies on biomolecular condensates focus on intrinsically disordered peptides derived from natural sequences, increasing evidence suggests that molecular ordering can play an important role in driving LLPS and condensate formation [27]. A systematic investigation of how structural ordering affects LLPS is therefore beneficial to advance mechanistic understanding and further expand the design space of synthetic peptides for constructing complex condensates. In this context, oligopeptides with β-sheet forming propensity offer a powerful model system for elucidating the influence of intermolecular interactions, such as directional hydrogen bond networks, π–π stacking, and hydrophobic effect on LLPS and complex coacervation. By systematically varying peptide length, amino acid chemistry, and assembly/disassembly domains, subtle changes in molecular design can be directly linked to differences in phase behavior, dynamics, and materials properties. It is worth noting that this approach is grounded in *de novo* peptide design with an inherent propensity to form β-sheet structures. A key question is to determine how enhanced molecular ordering, reflected by increased β-sheet content, can be effectively incorporated into biomolecular condensates. This approach differs from designs driven by IDP low complexity domains and sticker-spacer model [12, 17, 34], which typically lack well-defined secondary structures. Given the large existing repertoire of *de novo* designed peptides with β-sheet forming tendencies, this framework can be applied to these systems to provide a basis for engineering condensate-forming systems and to expand the design landscape beyond conventional IDP paradigms.

In this work, we evaluate our condensate design using modularly designed multidomain peptides (MDPs) with highly tunable secondary structures based on the design principle of molecular frustration [35]. Although MDPs were originally designed to form β-sheet hydrogels [36, 37], we show that through reprogramming of each domain and their frustration degree, a subset undergoes LLPS and recapitulates key features of biomolecular condensates. Their phase behavior is dictated by the secondary structure, which is encoded by the primary sequence and intermolecular interactions. Peptides remain soluble as a random coil conformation, form liquid droplets by enhanced intermolecular hydrogen bonding and hydrophobic effects, and transition to gels as β-sheet contents increase. Importantly, these condensates can be dynamically regulated by salts and synthetic anionic polymers. Complex coacervates are formed upon mixing MDPs with anionic polymers, such as polyglutamic acids (PGA) and the resulting condensates exhibit dramatically improved stability. Furthermore, we demonstrate that phosphorylated MDPs can form biomolecular condensates as triggered by alkaline phosphatase (ALP), a biomarker commonly overexpressed in bacterial infections and tumor microenvironments [38], highlighting the potential of these materials for bacterial imaging and antimicrobial applications.

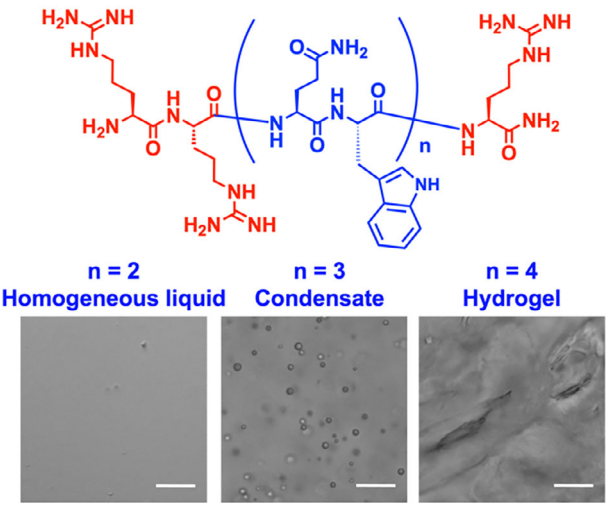

FIGURE 1 | Primary sequences of MDPs featuring variable numbers of QW repeating units and their resulting phase behaviors. Scale bar: 25 μm.

2 | Results and Discussion

2.1 | Design and Characterization of Condensate-forming MDPs

The MDP sequences used in the current study follow the same design principle of so-called molecular frustration (Table S1 and Figure S1) [35]. MDPs feature a central domain with alternating hydrophobic and hydrophilic residues that promote β-sheet self-assembly, flanked by cationic terminal domains that further modulate the assembly. By balancing these domains, intermolecular peptide interactions and resulting secondary structures can be systematically tuned. In this study, glutamine (Q) was chosen as the hydrophilic residue and tryptophan (W) as the hydrophobic residue within the central repeating domain while arginine (R) was selected in the terminal domain. Tryptophan was also selected due to recent findings in the design of condensate-forming peptides based on the sticker-spacer model, which highlights its frequent use [17, 26]. In the initial set of experiments, three peptides, denoted as $R_2(QW)_2R$, $R_2(QW)_3R$, and $R_2(QW)_4R$, were synthesized, in which the number of arginine residues was fixed at three while the number of central repeating units was varied from two to four (Figure 1).

All peptides were prepared in tris buffer (pH = 8, 50 mM) containing 800 mM of NaCl for initial screening of condensate formation and structural analysis. Circular dichroism (CD) spectroscopy showed that these peptides adopt distinct secondary structures, showing a clear structural transition from random coils to β-sheets as the number of QW repeating units increased (Figure 2a). For $R_2(QW)_3R$, partially folded β-sheets

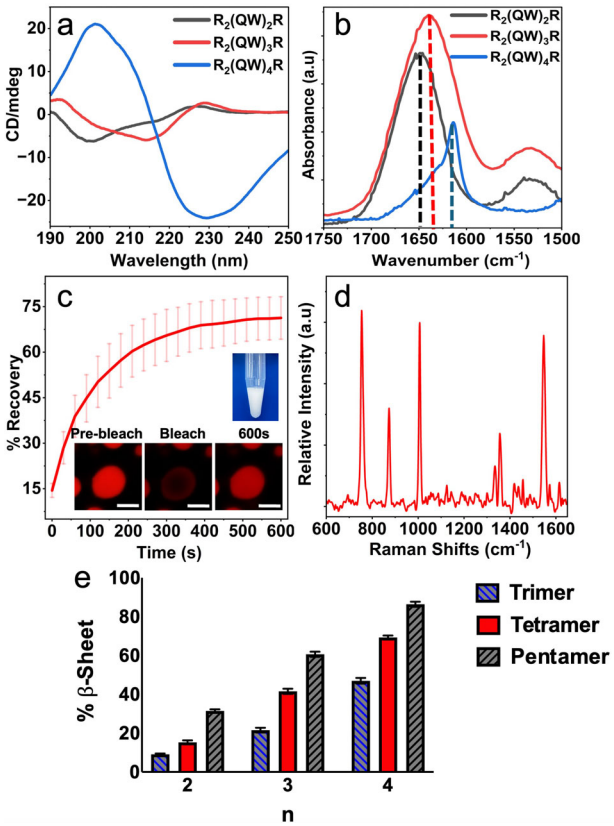

FIGURE 2 | (A) CD spectra of MDPs showing distinct secondary structures in Tris buffer (pH = 8, 50 mM) containing 800 mM NaCl. Peptide concentration: 5 mM. (B) FT-IR spectra of MDPs show a red shift of absorbance suggesting enhanced intermolecular hydrogen bonding as the number of QW repeating units increase. Samples at a concentration of 5 mM were prepared in D_2O containing 800 mM NaCl and pH was adjusted with NaOD. Samples were cast dried on an ATR plate for data acquisition. (C) FRAP data of freshly prepared $R_2(QW)_3R$ forming microdroplet condensates. Insets are confocal laser scanning microscopic pre-bleach and post-bleach images of rhodamine encapsulated droplets at time 0 and 600 s. Peptides were prepared in Tris buffer (pH = 8, 50 mM) containing 800 mM NaCl. Peptide concentration: 5 mM. Scale bar: 5 μm. (D) Confocal Raman spectrum of $R_2(QW)_3R$ forming microdroplet condensates. Samples were cast dried for data acquisition. Peptides were prepared in Tris buffer (pH = 8, 50 mM) containing 800 mM NaCl. Peptide concentration: 5 mM. (E) β-sheet percentage with different oligomer states and repeating units, n, for $R_2(QW)_nR$ peptides. The percentage of β-sheet secondary structure shown as a function of repeating units ($n = 2$, 3, 4), with the sequence of $R_2(QW)_nR$, assembled into trimers, tetramers, and pentamers. The error bars represent standard deviation across three independent replicates. β-sheet percentage composition was determined with DSSP analysis.

were observed given the double minimum at 200 and 215 nm. FT-IR spectroscopy further supported these findings, exhibiting a wavenumber shift from 1649 to to 1614 cm^{-1} in the amide I region as the peptides became more structurally ordered (Figure 2b). These molecular-level structural differences resulted in distinct phase behaviors at the microscopic level. $R_2(QW)_3R$ underwent LLPS and formed condensates, whereas $R_2(QW)_2R$ remained fully soluble and $R_2(QW)_4R$ gradually formed gels over time. Fluorescence recovery after photobleaching (FRAP) data confirmed the liquid-like nature of these droplets, as evidenced by fluorescence recovery within minutes (Figure 2c and insets). Confocal Raman microscopy provided further insights into the underlying molecular interactions for condensate formation of $R_2(QW)_3R$ in which tryptophan residues have specific Raman fingerprints (Figure 2d) [9, 39]. Notably, the peak observed at 875 cm^{-1} suggests the hydrogen bonding interaction between the NH group on the indole ring with medium. The Fermi doublet associated with tryptophan were observed at 1360 and 1340 cm^{-1}. The larger peak ratio of I_{1360}/I_{1340} supports strong hydrophobic interaction involved in condensate formation. The 1008 cm^{-1} is attributed to van der Waals interaction of the indole ring of tryptophan with surrounding residues. Furthermore, substitution of a single arginine with lysine inhibited LLPS and instead promoted hydrogel formation presumably due to the enhanced crosslinking capability of lysine residues (Table S1 and Figure S2). Reducing the number of arginine residues also abolished LLPS as the balance shifted toward self-assembly as driven by the central domain. For example, $R(QW)_3R$ self-assembled into β-sheet hydrogels upon salt addition (Table S1 and Figure S3). Molecular dynamic (MD) simulations were performed to investigate the effect of QW repeating units on β-sheet propensity of the peptides. Three independent MD production simulations were conducted for $R_2(QW)_2R$, $R_2(QW)_3R$, $R_2(QW)_4R$ with different oligomerization states, including trimers, tetramers, and pentamers, respectively (Figure S4 and Table S2). Dimers were excluded due to their limited structural stability and inability to capture the cooperative intermolecular interactions associated with peptide aggregation [40]. Define secondary structure of proteins (DSSP) analysis showed that β-sheet content increased with both QW repeating units and the degree of oligomer states (Figure 2e and Table S3). For example, with the trimer assemblies, β-sheet contents increased from 9.1% for $R_2(QW)_2R$ to 47.0% for $R_2(QW)_4R$. Similar trends were observed for tetramers and pentamers indicating enhanced intermolecular β-sheet stabilization with increasing peptide length and oligomerization state. In contrast, random coil content progressively decreased, while no α-helical structures were observed in any simulations. It is worth noting that these computation result may not define the exact β-sheet content required to form condensates and residue-specific molecular conformations remain to be fully resolved through more detailed high resolution experimental and computation studies. Nevertheless, the preliminary MD simulations suggest that increasing the QW repeating units promotes intermolecular β-sheet formation and structural ordering within the peptide assemblies.

2.2 | Effect of Hydrophobic Residue Substitution on Peptide Secondary Structures and Phase Behaviors

Based on the structural analysis on $R_2(QW)_3R$, we hypothesize that the partially folded β-sheets play a key role in the formation of condensates. As the next step, the central tryptophan residue in the $(QW)_3$ domain was substituted with tyrosine (Y), phenylalanine (F), leucine (L), and alanine (A) to investigate the effect of aromatic and aliphatic residues on secondary structures and phase behaviors (Table S1). These peptides are denoted as QY, QF, QL and QA, respectively (Figure 3a). All peptides were initially screened for condensation in Tris buffer containing

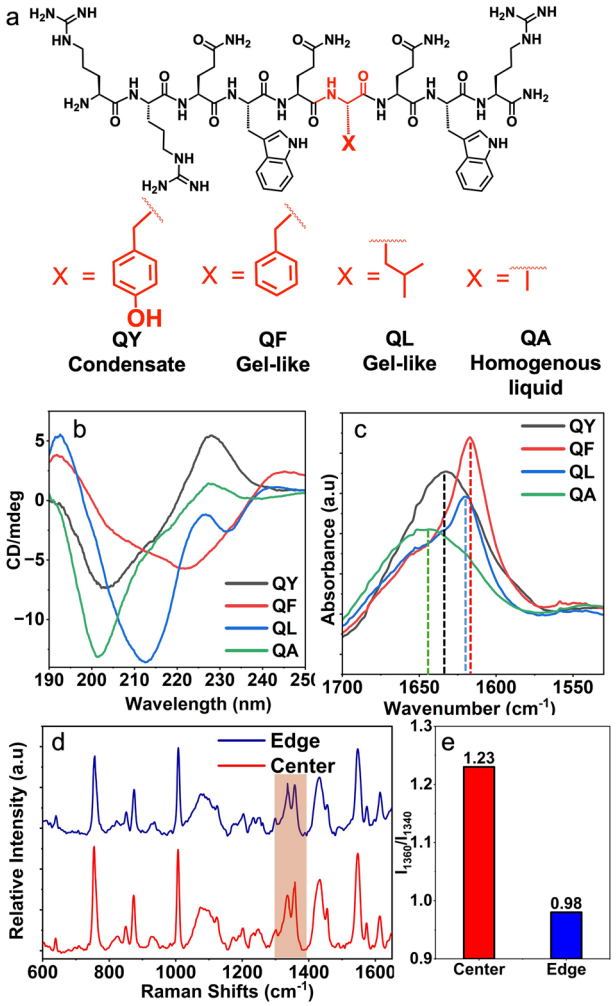

FIGURE 3 | (A) Primary structures of MDP variants by substituting W with Y, F, L, and A and the resulting phase behaviors. (B) CD spectra of QY, QF, QL, and QA showing distinct secondary structures in tris buffer (pH = 8, 50 mM) containing 800 mM NaCl. Concentration of QY and QA: 10 mM; Concentration of QF and QL: 5 mM. (C) FT-IR spectra of QY, QF, QL and QA. Samples were prepared in D_2O with NaCl (final conc: 800 mM). pH was adjusted with NaOD to reach a final pH at 8. Samples were cast dried on an ATR plate for data acquisition. (D) Confocal Raman spectra of condensates formed by QY. Samples were cast dried on a glass slide. Measurements were conducted in the center and edge regions. (E) Comparison of the peak ratio of I_{1360}/I_{1340} taken for condensates formed by QY in the center and edge regions.

800 mM NaCl. Experimental results showed that QY instantaneously formed condensates whereas QF and QL formed viscous gel-like solutions and QA remains as homogeneous liquid. CD analysis showed that QA adopted a random coil conformation, whereas QF and QL exhibited β-sheet rich secondary structures. In contrast, QY displayed a partially folded β-sheet as indicated by the shoulder peak at 215 nm (Figure 3b). Consistent with the CD results, FT-IR spectroscopy provided further evidence that increased molecular ordering drives peptide organization from liquids to condensates and ultimately gel-like structures as indicated by the shift of the amide I absorption to lower wavenumbers (Figure 3c). Together, these results indicate that while hydrophobic residues could drive peptide chain association through hydrophobic effects, hydrogen bonding plays a critical role in stabilizing peptides in the condensate states.

Given that condensates exhibit liquid-like and highly dynamic properties, we further investigated the secondary structures of QY under both salt-free solution conditions and conditions that promote condensate formation (QY at 10 mM in Tris with 800 mM NaCl) using solution-state NMR spectroscopy. However, under condensate-forming conditions, the NMR signals became significantly broad and difficult to resolve. To address this, measurements were instead conducted at concentrations just below the critical condensation concentration to allow assessment of salt-induced conformational changes. Based on the 1D ^{1}H-NMR and 2D COSY spectra (Figure S5), all α-protons were identified in the range of 3.30 to 4.56 ppm (Table S4). Upon salt addition, a downfield shift was observed for all α-protons with the most pronounced change (0.13 ppm) detected for the tyrosine α-proton (Figure S6), indicating a local change in secondary structural propensity toward β-strand formation [41]. The α-protons of glutamine and arginine residues also showed downfield shifts, although to a lesser extent (0.05–0.08 ppm) (Figure S6 and Table S5). Although α-protons of tryptophan residues were obscured by the solvent signal, a clear downfield shift was still evident when comparing salt-free and high salt conditions. While solid-state NMR spectroscopy will be required to definitively confirm secondary structure rearrangement in the condensate phase and to resolve molecular packing within condensates, the overall changes observed in the solution-state NMR consistently suggested increased molecular ordering upon salt addition. Furthermore, comprehensive characterization of QY was performed using confocal Raman microscopy (Figure 3d,e). Dried droplets upon condensation were prepared on a glass slide and spectra were collected focusing on the edge and interior regions, respectively. Although most Raman peaks remained largely unchanged between these regions, a drastic increase in the I_{1360}/I_{1340} ratio from 0.98 at the edge to 1.23 in the interior was observed. The increased ratio in the center region suggests enhanced hydrophobic effects and their critical role in driving LLPS and condensation [9, 39]. The possibility of cation–π interactions is particularly intriguing as they have been reported to drive condensation in several peptide-based systems [17, 26]. To probe their role in the MDP system, we synthesized a QY variant in which the arginine residues were replaced with monomethylated arginine, denoted as QY-R(Me). Condensation was still observed under the same conditions as for QY. Notably, both peptides undergo phase separation at relatively high salt concentrations rather than under physiological conditions. Furthermore, Raman mapping showed that the 700–800 cm^{-1} region, which is attributed to cation–π interaction, exhibited negligible peak shifts (~1 cm^{-1}) between the center and edge of condensates. This subtle change suggests that cation–π interactions may play a relatively minor role in this system. The primary driving forces are more likely dominated by hydrophobic effects and π–π stacking further reinforced by hydrogen bonding among tyrosine residues.

2.3 | Formation of Complex Condensates with Anionic Polymers

Initial screening of peptides for self-condensation serves as a useful approach to identify sequences capable of forming

condensates. In addition, self-condensates allow systematic spectroscopic characterization without interference from additional synthetic components. However, self-coacervates formed by the QY peptide require very high concentrations to undergo LLPS, and the resulting microdroplets are only transiently stable before reverting to the homogeneous liquid state within ~30 min, limiting their utility for practical applications. To address this limitation, the incorporation of anionic polymers was explored as a strategy to reduce the critical concentration required for condensation and to enhance stability through multivalent electrostatic interactions for practical applications. For this purpose, PGA (15–50 kDa) was used as model synthetic anionic polymers to form complex coacervates with QY. PGA effectively induced LLPS and promoted QY condensation with the resulting microdroplets exhibiting rapid fluorescence recovery in FRAP experiments (Figure S7). The condensates persisted at 37°C for 48 h as determined by UV–Vis turbidity measurements (using an OD cut-off of 1.0) (Figure S8) and optical microscopy (Figure S9). To examine the thermodynamics of the condensation between QY and PGA, isothermal titration calorimetry (ITC) was conducted by titrating PGA into QY. The charge concentration for both molecules were considered in the analysis. The resulting thermogram clearly demonstrated a saturable, exothermic interaction (Figure S10). Fitting the data using a simple, 1:1 model with the concentration of QY adjusted by a factor N [42] yielded a dissociation constant (K_D) of 80 μM, ΔH of -2.25 kcal mol^{-1} and a charge binding ratio N of 1.39 (PGA to QY). Based on these values, ΔS was calculated to be 11.0 cal mol^{-1} K^{-1}, indicating both enthalpy and entropy make contributions to the overall free energy of condensation process.

2.4 | In situ Triggered Condensate Formation

To further evaluate condensation capability under biologically relevant conditions, we designed an experiment that allows *in situ* peptide condensation in response to a disease-associated stimulus. As a proof-of-concept design, ALP was selected as the trigger due to its elevated activity in many pathogenic bacteria and infected tissues [43–45]. This design links enzymatic activity directly to condensate formation. For these studies, a peptide containing two phosphorylated tyrosine residues, denoted QY(2P), was synthesized. Phosphorylation completely suppressed LLPS when QY(2P) was mixed with PGA in Tris buffer. We next investigated whether ALP could restore condensation of QY(2P) in the presence of PGA. As shown in Figure S11, condensates were formed upon addition of ALP to QY(2P)/PGA solutions. Mass spectrometry further confirmed that dephosphorylation occurred in solution (Figure S12). Finally, ALP triggered condensation was evaluated in a bacterial culture model using methicillin-resistant *Staphylococcus aureus* (MRSA). QY(2P) alone and QY(2P)/PGA formulations were prepared, each containing 0.1% of rhodamine labeled QY(2P) for fluorescence visualization. The samples were added into SYTO-9-stained MRSA cultures with and without exogenous ALP, where live bacteria appeared green under fluorescence imaging. In the absence of exogenous ALP, negligible rhodamine fluorescence was observed due to diffusion of the free peptide throughout the culture medium (Figure 4a,c). In contrast, distinct condensates were formed in the presence of ALP (Figure 4b,d). Although QY(2P) alone underwent ALP-triggered LLPS possibly due to interactions with negatively charged bacterial membrane components, the resulting self-coacervates were less stable than the complex coacervates formed with PGA. After 24 h incubation with MRSA, complex coacervates are predominant whereas only limited quantities of self-coacervates persisted (Figure S13). Furthermore, reduced bacterial viability was observed in both ALP-treated cultures containing either self-condensates or complex condensates (Figure 4b,d). The observed bactericidal activity is likely attributed to the antimicrobial nature of the multidomain peptides, which mimic the amphiphilic structure of natural antimicrobial peptides. Detailed antimicrobial investigations will be the focus of future studies. In this context, the *in situ* formed condensates are expected to undergo sustained release of antimicrobial peptides as well as potentially encapsulated antibiotics for synergic antimicrobial therapy.

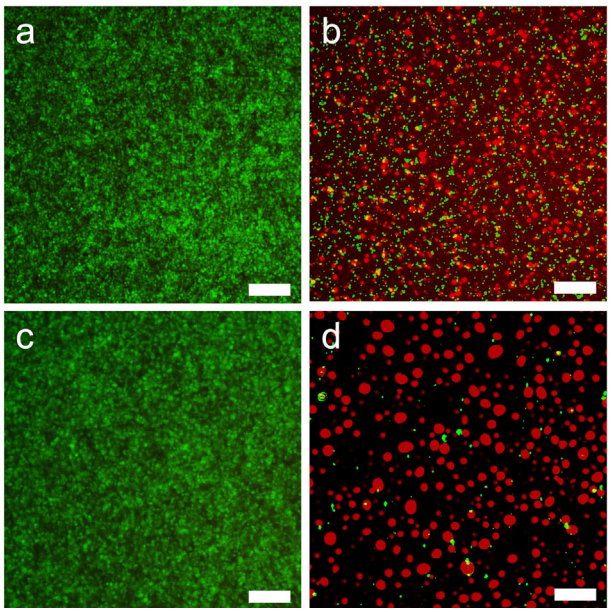

FIGURE 4 | Fluorescence images of MRSA treated with (A) QY(2P) w/o ALP. (B) QY(2P) with ALP. (C) QY(2P)/PGA (1:0.2) w/o ALP. (D) QY(2P)/PGA (1:0.2) with ALP. All samples were incubated with MRSA for 4 h and condensates are shown in red containing rhodamine labelled peptides. MRSA were stained with SYTO-9 for visualization of live bacteria in green. Scale bar: 25 μm.

3 | Conclusion

In summary, we demonstrated a class of MDPs with modularly designed assembly and disassembly domains based on the design principle of molecular frustration. Although MDPs were primarily used in the construction of β-sheet nanofiber hydrogels, we found that a subset of MDPs underwent LLPS and condensate formation is driven by partially ordered secondary structures. Compared with existing peptide condensates that are mostly driven by natural or synthetic IDPs, MDPs are designed through *de novo* with a more systematic control over molecular structure and ordering and therefore the driving force toward condensates formation. Indeed, the modularity and versatility of the sequence design enable the construction of complex condensates and enzyme-triggered condensates in the presence of bacteria. The current work laid out a foundation for the design and synthesis MDP-based biomolecular

condensates and complex coacervate materials toward a range of applications.

Acknowledgements

This study was supported by the National Science Foundation (DMR 2341925), the National Science Foundation Partnership for Research and Education in Functional Materials under the award DMR 2425164). This work was partially supported by the National Institutes of Health (NIH) under Award No. R15GM122013 to Peng Tao. This work made use of the SPID facilities of the NUANCE Center at Northwestern University which has received support from the Soft and Hybrid Nanotechnology Experimental (SHyNE) Resource (NSF ECCS-2025633), MRSEC program (NSF DMR-2308691) at the Materials Research Center, the International Institute for Nanotechnology (IIN), the Keck Foundation, and the State of Illinois through the IIN. We acknowledge Dr. Brian Edwards for his assistance with the NMR experiments and valuable discussions.

Conflicts of Interest

The authors declare no conflict of interest.

Data Availability Statement

The data that support the findings of this study are available in the Supporting Information.

References

1. P. Li, S. Banjade, H.-C. Cheng, et al., "Phase Transitions in the Assembly of Multivalent Signalling Proteins," *Nature* 483 (2012): 336–340, https://doi.org/10.1038/nature10879.

2. Y. Shin and C. P. Brangwynne, "Liquid Phase Condensation in Cell Physiology and Disease," *Science* 357 (2017): aaf4382.

3. M. Feric, N. Vaidya, T. S. Harmon, et al., "Coexisting Liquid Phases Underlie Nucleolar Subcompartments," *Cell* 165 (2016): 1686–1697, https://doi.org/10.1016/j.cell.2016.04.047.

4. C. P. Brangwynne, C. R. Eckmann, D. S. Courson, et al., "Germline P Granules Are Liquid Droplets That Localize by Controlled Dissolution/Condensation," *Science* 324 (2009): 1729–1732, https://doi.org/10.1126/science.1172046.

5. S. Jain, J. R. Wheeler, R. W. Walters, A. Agrawal, A. Barsic, and R. Parker, "ATPase-Modulated Stress Granules Contain a Diverse Proteome and Substructure," *Cell* 164 (2016): 487–498, https://doi.org/10.1016/j.cell.2015.12.038.

6. D. L. J. Lafontaine, J. A. Riback, R. Bascetin, and C. P. Brangwynne, "The Nucleolus as a Multiphase Liquid Condensate," *Nature Reviews Molecular Cell Biology* 22 (2021): 165–182, https://doi.org/10.1038/s41580-020-0272-6.

7. S. F. Banani, H. O. Lee, A. A. Hyman, and M. K. Rosen, "Biomolecular Condensates: Organizers of Cellular Biochemistry," *Nature Reviews Molecular Cell Biology* 18 (2017): 285–298, https://doi.org/10.1038/nrm.2017.7.

8. R. Harris, N. Berman, and A. Lampel, "Coacervates as Enzymatic Microreactors," *Chemical Society Reviews* 54 (2025): 4183–4199, https://doi.org/10.1039/D4CS01203H.

9. L. Zhou, L. Zhu, C. Wang, et al., "Multiphasic Condensates Formed With Mono-Component of Tetrapeptides via Phase Separation," *Nature Communications* 16 (2025): 2706, https://doi.org/10.1038/s41467-025-58060-6.

10. M. Dzuricky, B. A. Rogers, A. Shahid, P. S. Cremer, and A. Chilkoti, "De Novo Engineering of Intracellular Condensates Using Artificial Disordered Proteins," *Nature Chemistry* 12 (2020): 814–825, https://doi.org/10.1038/s41557-020-0511-7.

11. D. Priftis, N. Laugel, and M. Tirrell, "Thermodynamic Characterization of Polypeptide Complex Coacervation," *Langmuir* 28 (2012): 15947–15957, https://doi.org/10.1021/la302729r.

12. M. Abbas, W. P. Lipinski, K. K. Nakashima, W. T. S. Huck, and E. Spruijt, "A Short Peptide Synthon for Liquid–liquid Phase Separation," *Nature Chemistry* 13 (2021): 1046–1054, https://doi.org/10.1038/s41557-021-00788-x.

13. H. Fu, J. Huang, J. J. B. van der Tol, et al., "Supramolecular Polymers Form Tactoids Through Liquid–liquid Phase Separation," *Nature* 626 (2024): 1011–1018, https://doi.org/10.1038/s41586-024-07034-7.

14. C. E. Sing and S. L. Perry, "Recent Progress in the Science of Complex Coacervation," *Soft Matter* 16 (2020): 2885–2914, https://doi.org/10.1039/D0SM00001A.

15. L. Leon, G. M. Santiago, and E. Spruijt, "Coacervation in Systems Chemistry," *Communications Chemistry* 7 (2024): 275, https://doi.org/10.1038/s42004-024-01358-1.

16. F. P. Cakmak, S. Choi, M. O. Meyer, P. C. Bevilacqua, and C. D. Keating, "Prebiotically-Relevant Low Polyion Multivalency Can Improve Functionality of Membraneless Compartments," *Nature Communications* 11 (2020): 5949, https://doi.org/10.1038/s41467-020-19775-w.

17. A. Baruch Leshem, S. Sloan-Dennison, T. Massarano, et al., "Biomolecular Condensates Formed by Designer Minimalistic Peptides," *Nature Communications* 14 (2023): 421, https://doi.org/10.1038/s41467-023-36060-8.

18. Y. Sun, S. Y. Lau, Z. W. Lim, et al., "Phase-Separating Peptides for Direct Cytosolic Delivery and Redox-Activated Release of Macromolecular Therapeutics," *Nature Chemistry* 14 (2022): 274–283, https://doi.org/10.1038/s41557-021-00854-4.

19. W. M. Aumiller Jr and C. D. Keating, "Phosphorylation-Mediated RNA/Peptide Complex Coacervation as a Model for Intracellular Liquid Organelles," *Nature Chemistry* 8 (2016): 129–137, https://doi.org/10.1038/nchem.2414.

20. A. Netzer, I. Katzir, A. Baruch Leshem, M. Weitman, and A. Lampel, "Emergent Properties of Melanin-Inspired Peptide/RNA Condensates," *Proceedings of the National Academy of Sciences* 120 (2023): 2310569120, https://doi.org/10.1073/pnas.2310569120.

21. C. Forenzo and J. Larsen, "Complex Coacervates as a Promising Vehicle for mRNA Delivery: A Comprehensive Review of Recent Advances and Challenges," *Molecular Pharmaceutics* 20 (2023): 4387–4403, https://doi.org/10.1021/acs.molpharmaceut.3c00439.

22. J. Wang, M. Abbas, J. Wang, and E. Spruijt, "Selective Amide Bond Formation in Redox-Active Coacervate Protocells," *Nature Communications* 14 (2023): 8492, https://doi.org/10.1038/s41467-023-44284-x.

23. M. Abbas, W. P. Lipinski, J. Wang, and E. Spruijt, "Peptide-Based Coacervates as Biomimetic Protocells," *Chemical Society Reviews* 50 (2021): 3690–3705, https://doi.org/10.1039/D0CS00307G.

24. W. Wang and J. Shi, "Peptides for Liquid-Liquid Phase Separation: An Emerging Biomaterial," *ChemBioChem* 26 (2025): 202400773, https://doi.org/10.1002/cbic.202400773.

25. A. Netzer, A. Baruch Leshem, S. Veretnik, I. Edelstein, and A. Lampel, "Regulation of Peptide Liquid–Liquid Phase Separation by Aromatic Amino Acid Composition," *Small* 20 (2024): 2401665, https://doi.org/10.1002/smll.202401665.

26. V. Castelletto, J. Seitsonen, A. Pollitt, and I. W. Hamley, "Minimal Peptide Sequences That Undergo Liquid–Liquid Phase Separation via Self-Coacervation or Complex Coacervation With ATP," *Biomacromolecules* 25 (2024): 5321–5331, https://doi.org/10.1021/acs.biomac.4c00738.

27. L. Zhou, L. Lu, Y. Zhang, J. Wang, J. Cheng, and H. Wang, "Water Dynamics in the Formation of Single-Component-Based Multiphasic Droplets," *Journal of the American Chemical Society* 147 (2025): 31290–31299, https://doi.org/10.1021/jacs.5c10784.

28. S. Cao, P. Zhou, G. Shen, et al., "Binary Peptide Coacervates as an Active Model for Biomolecular Condensates," *Nature Communications* 16 (2025): 2407, https://doi.org/10.1038/s41467-025-57772-z.

29. J. Lim, A. Kumar, K. Low, et al., "Liquid–Liquid Phase Separation of Short Histidine- and Tyrosine-Rich Peptides: Sequence Specificity and Molecular Topology," *The Journal of Physical Chemistry B* 125 (2021): 6776–6790, https://doi.org/10.1021/acs.jpcb.0c11476.

30. D. Q. Reis, S. Pereira, A. P. Ramos, et al., "Catalytic Peptide-Based Coacervates for Enhanced Function Through Structural Organization and Substrate Specificity," *Nature Communications* 15 (2024): 9368, https://doi.org/10.1038/s41467-024-53699-z.

31. Q. Guo, G. Zou, X. Qian, et al., "Hydrogen-Bonds Mediate Liquid-Liquid Phase Separation of Mussel Derived Adhesive Peptides," *Nature Communications* 13 (2022): 5771, https://doi.org/10.1038/s41467-022-33545-w.

32. C. M. Green, D. Sementa, D. Mathur, et al., "Sequestration Within Peptide Coacervates Improves the Fluorescence Intensity, Kinetics, and Limits of Detection of Dye-Based DNA Biosensors," *Communications Chemistry* 7 (2024): 49, https://doi.org/10.1038/s42004-024-01124-3.

33. V. Castelletto, L. de Mello, J. Seitsonen, and I. W. Hamley, "Fibrillization versus Coacervation in Arginine–tryptophan Repeat Peptides: Effects of Sequence Length and pH," *Materials Advances* 6 (2025): 8670–8685, https://doi.org/10.1039/D5MA01006C.

34. S. Cao, G. Li, P. Zhou, E. Gazit, X. Yan, and C. Yuan, "Entropy-Driven Amino Acid-Based Coacervates With Enzyme-Free Metabolism and Prebiotic Robustness," *Journal of the American Chemical Society* 147 (2025): 45324–45336, https://doi.org/10.1021/jacs.5c15328.

35. H. Dong, S. E. Paramonov, L. Aulisa, E. L. Bakota, and J. D. Hartgerink, "Self-Assembly of Multidomain Peptides: Balancing Molecular Frustration Controls Conformation and Nanostructure," *Journal of the American Chemical Society* 129 (2007): 12468–12472, https://doi.org/10.1021/ja072536r.

36. L. Jiang, D. Xu, T. J. Sellati, and H. Dong, "Self-Assembly of Cationic Multidomain Peptide Hydrogels: Supramolecular Nanostructure and Rheological Properties Dictate Antimicrobial Activity," *Nanoscale* 7 (2015): 19160–19169, https://doi.org/10.1039/C5NR05233E.

37. H. Asokan-Sheeja, K. Awad, J. Xu, et al., "In Situ Synthesis and Self-Assembly of Peptide–PEG Conjugates: A Facile Method for the Construction of Fibrous Hydrogels," *Biomacromolecules* 25 (2024): 2814–2822, https://doi.org/10.1021/acs.biomac.3c01450.

38. J. Zhang, Y. Fu, R. Zhou, et al., "The Construction of Alkaline Phosphatase-Responsive Biomaterial and Its Application for in Vivo Urinary Tract Infection Therapy," *Advanced Healthcare Materials* 12 (2023): 2202421, https://doi.org/10.1002/adhm.202202421.

39. H. Takeuchi, "Raman Structural Markers of Tryptophan and Histidine Side Chains in Proteins," *Biopolymers* 72 (2003): 305–317, https://doi.org/10.1002/bip.10440.

40. J. Razzokov, S. Naderi, and P. Van Der Schoot, "Nanoscale Insight Into Silk-Like Protein Self-Assembly: Effect of Design and Number of Repeat Units," *Physical Biology* 15 (2018): 066010, https://doi.org/10.1088/1478-3975/aadb5e.

41. D. S. Wishart, C. G. Bigam, A. Holm, R. S. Hodges, and B. D. Sykes, "1H, 13C and 15N Random Coil NMR Chemical Shifts of the Common Amino Acids. I. Investigations of Nearest-Neighbor Effects," *Journal of Biomolecular NMR* 5 (1995): 67–81, https://doi.org/10.1007/BF00227471.

42. T. Wiseman, S. Williston, J. F. Brandts, and L.-N. Lin, "Rapid Measurement of Binding Constants and Heats of Binding Using a New Titration Calorimeter," *Analytical Biochemistry* 179 (1989): 131–137, https://doi.org/10.1016/0003-2697(89)90213-3.

43. M. Hughes, S. Debnath, C. W. Knapp, and R. V. Ulijn, "Antimicrobial Properties of Enzymatically Triggered Self-Assembling Aromatic Peptide Amphiphiles," *Biomaterials Science* 1 (2013): 1138, https://doi.org/10.1039/c3bm60135h.

44. E. B. Kang, Z. A. I. Mazrad, A. I. Robby, I. In, and S. Y. Park, "Alkaline Phosphatase-Responsive Fluorescent Polymer Probe Coated Surface for Colorimetric Bacteria Detection," *European Polymer Journal* 105 (2018): 217–225, https://doi.org/10.1016/j.eurpolymj.2018.05.035.

45. S. B. Singh and H. C. Lin, "Role of Intestinal Alkaline Phosphatase in Innate Immunity," *Biomolecules* 11 (2021): 1784, https://doi.org/10.3390/biom11121784.

Supporting Information

Additional supporting information can be found online in the Supporting Information section.

Supporting File: smll74434-sup-0001-SuppMat.pdf.